Application of Modal Testing and Analysis Techniques on a sUAV

Kaci J. Lemler and William H. Semke
Unmanned Aircraft Systems Engineering Laboratory
School of Engineering and Mines
University of North Dakota
Grand Forks, ND 58202

ABSTRACT
This paper's focus is on experimental structural analysis using contemporary testing techniques for a small unmanned aerial vehicle (sUAV). Testing was performed to find the bending and torsional modes of the wings and tail utilizing multiple methods. Data acquisition and analysis were performed using ModalVIEW, a structural analysis program supported by LabVIEW. The aircraft was excited with random excitation using a single mechanical shaker. These techniques were applied in a case study on the BTE Super Hauler airframe, a small UAS operated by the Unmanned Aircraft Systems Engineering (UASE) Laboratory at the University of North Dakota. The aircraft is primarily used for flight testing of multiple payloads, including an antenna system designed for use in sense and avoid applications. This application requires the addition of wing pods to the current airframe to avoid electro-magnetic interference from the engine of the UAS. Therefore, the effects of the two wing pods on the structural dynamic behavior of the UAS, as well as flutter analysis, were performed on the aircraft and the results are presented and compared. In addition, a statistical method of critical sensor placement for accurate modal information with limited accelerometers is discussed.

Keywords: Modal Analysis, Unmanned Aerial Vehicle, Sensor Placement, Flutter Analysis, ModalVIEW

INTRODUCTION
Modal analyses were performed on a small Unmanned Aircraft Systems (UAS) both with and without wing pods and the results were compared to find the effect the wing pods have on the structural characteristics of the aircraft. A study on channel reduction was also performed and a novel sensor location identification method using a laser vibrometer was developed. Finally, the results were examined to determine the airworthiness of the aircraft with the wing pods installed.

As UAS are being integrated into the National Air Space (NAS) it is important that steps be taken to develop and implement sense and avoid systems into said UAS [1]. These systems are necessary to enable UAS to sense and avoid obstacles such as uncooperative aircraft, birds, power lines, buildings, and other obstacles [2]. The Unmanned Systems Aircraft Engineering (UASE) team at the University of North Dakota has done work in the field of sense and avoid systems for small UAS. One system that was developed uses an Automatic Dependent Surveillance-Broadcast (ADS-B) transponder to track cooperative aircraft that also have ADS-B transponders. This system works well to predict and avoid collision scenarios with cooperative aircraft but doesn't assist in sense and avoid applications for uncooperative obstacles. Therefore, work is also being done on a small phased array radar system that can be installed into the small UAS along with the ADS-B to provide the ability to track cooperative and uncooperative obstacles. This phased array radar system includes an antenna that locates objects by radiating a narrow beam of electromagnetic energy in the direction of interest. This beam is also steerable so that it can locate objects at all locations around the UAS [2]. Because this antenna radiates electromagnetic energy, it needs to have a clear field of view, containing no metal components, between it and its target [3]. This introduces a need to mount the antennas on the wings to eliminate the engine, landing gear, and assorted fuselage components that could block the view of the antennas if they were mounted in the fuselage. The use of wing pods eliminates any unwanted view interference and provides a payload bay on the wings in which to mount the antennas. The wing pods can dramatically change the structural and flight characteristics of the aircraft, making a experimental structural analysis study necessary to prove airworthiness of the modified aircraft.

The UASE team consists of a mix of undergraduate and graduate students in Mechanical Engineering and Electrical Engineering. The purpose of the lab is to design, build, and flight test payloads for UAS. UASE has performed over 80 missions and has developed payloads relating to phased array radar, search and rescue, precision agriculture, sense and avoid, laser communications, and more. Flight testing is performed at Camp Grafton South, a military training facility in central North Dakota. This facility has restricted airspace, allowing UASE to safely and legally operate its UAS fleet. UASE owns and operates multiple UAS, one of which is the Bruce Tharpe Engineering Super Hauler, (henceforth referred to as the Super Hauler). The Super Hauler the red and white aircraft on the right in Figure 1 and is a gas powered UAS constructed of plywood, balsa wood, and Monokote. It has a 12 foot wingspan and a dry weight of 48 pounds. The engine is a 2-cylinder, 9.8 horsepower engine. The Super Hauler is capable of carrying payloads that weigh up to 30 pounds and has an electromagnetic shielded payload bay measuring 21 inches by 11 inches by 12 inches.

Figure 1. Unmanned Aircraft System Engineering team with the UAS they operate.

TEST OVERVIEW

The structural modes and natural frequencies of a structure can be obtained through ground vibration tests (GVTs). Ground vibration tests are important tests to perform on an aircraft as they are used to predict flutter and asses the significance of modifications made to the structure [4]. The main tool used in a GVT is the frequency response function (FRF). This function can be based on the displacement, velocity, or acceleration response of a system [5]. The expression for any FRF can be written as

$$H_{jk}(\omega) = \frac{X_j}{F_k} \tag{1}$$

where X_j is the harmonic response in one of the degrees of freedom, j, caused by F_k which is a harmonic force at a different degree of freedom, k [6]. Modal analysis is performed by curve-fitting the FRF obtained from the testing to obtain modes then applying that data to a model of the structure to find the associated mode shapes.

As stated previously, modal analyses on the Super Hauler were made necessary by the addition of wing pods. The wing pods used to hold the antennas were designed and built by members of UASE. The pods are made entirely of polycarbonate to eliminate any electromagnetic interference [3]. The aerodynamic shape of the pods results in less drag thus decreasing the effect of the pods on flight performance. The payload pods mount at the intersections of the wing segments using an aluminum mounting rib that follows the contour of the wing at this location. The overall dimensions of the pods are 7.75 inches long by 11 inches wide by 2.5 inches deep and each pod can carry up to 5 pounds. The pods will most often be used in pairs to equalize the wing loading and provide a symmetric load on the airframe. The electrical and power connectors and wiring are run inside of the wing to keep them out of the airflow over the wing. Figure 2 shows the wing pods mounted on the Super Hauler.

Figure 2. Wing payload pod on the Super Hauler.

For the modal testing, the Super Hauler was isolated by suspending it on bungee cords in a test rig so that all the wheels were 1.25 inches off of the ground. This setup simulates a free-free boundary condition. The Super Hauler was then instrumented with uni-axial and tri-axial accelerometers in key locations. The instrumented Super Hauler in the test rig can be seen in Figure 3. Tests were performed with and without the wing pods installed. For all of the tests with the pods, weight was added to the pods so that a total weight of 5 pounds was attached to each wing. There was no payload in the payload bay during the testing.

Figure 3. The Super Hauler in the test rig while instrumented with accelerometers.

Excitation of the Super Hauler was achieved by a small shaker. The shaker that was used was the Mini SmartShaker™ with an integrated power amplifier from The Modal Shop Inc. The setup of the shaker can be seen in Figure 4a where it was attached to the aircraft through the use of a suction cup. A load cell was attached in line with the shaker's stinger to measure input force. The aircraft was excited at several different locations, all in the Z direction, that are identified by the red dots in Figure 4b.

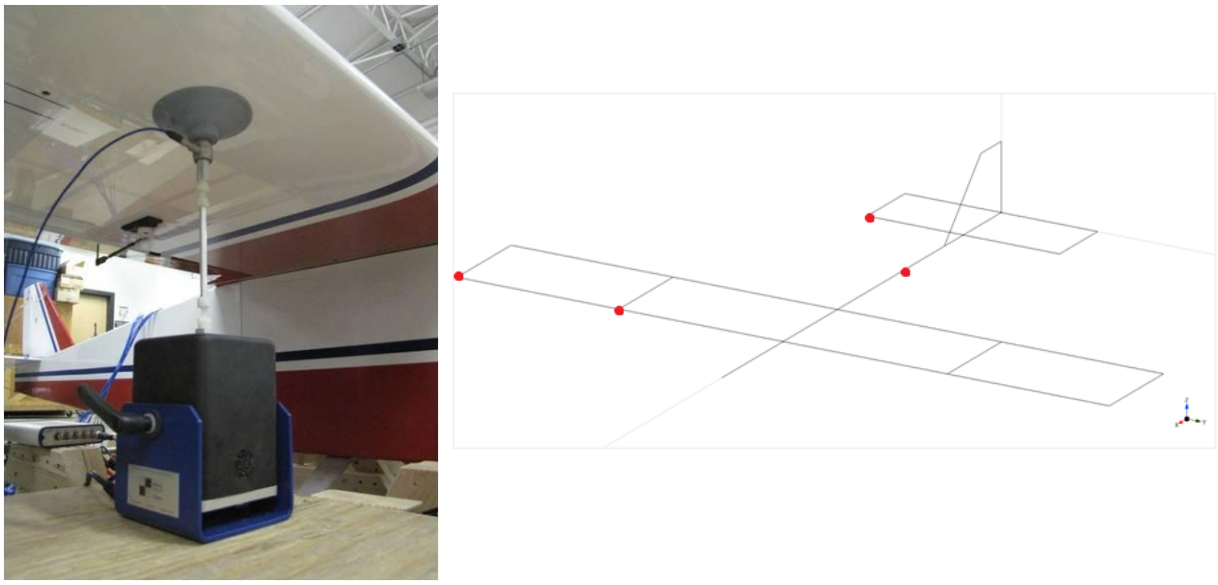

(a) (b)

Figure 4. (a) The shaker setup with stinger, load cell, and suction cup (b) Excitation locations.

The accelerometers and excitation devices were routed to a National Instruments data acquisition board that was connected directly to a computer. The DAQ that was used was a National Instruments cDAQ-9178 with eight National Instruments 9234 DAQ modules installed. This setup can be seen in Figure 5.

Figure 5. National Instruments cDAQ-9178 data acquisition board used for the testing

Table 1. Test equipment information.

Description	Model	Sensitivity
Uni-axial Accelerometer	PCB Piezotronics 352C18	10 mV/g
Uni-axial Accelerometer	PCB Piezotronics 352C33	100 mV/g
Tri-axial Accelerometer	PCB Piezotronics 356A32	100 mV/g
Load Cell	PCB Piezotronics 208C02	50 mV/g
Shaker	The Modal Shop Inc. K2007E01	
Data Acquisition Board	National Instruments cDAQ-9178	
Data Acquisition Modules	National Instruments 9234	

Data capture and analysis was performed using ModalVIEW, a software designed specifically for modal testing and analysis. The settings in ModalVIEW were as follows. The shaker was set to random excitation with a Hanning window applied. The measurement type was set to FRF-EMA for an experimental modal analysis. The sampling rate was left at the default of 1651.61 Hz and the resolution was set to 0.1 Hz. The shaker was activated so that the Super Hauler was excited with random excitation, then ModalVIEW was told to record data from the accelerometers. ModalVIEW would then gather data for a period of time and when it was done the shaker was turned off. This was repeated so that two data sets were gathered at each loading and excitation configuration then the shaker was moved to the next excitation location and the process was rerun.

Once all of the vibration data was gathered, analysis was performed using ModalVIEW and followed the steps outlined below. First, ModalVIEW automatically generated a frequency response function (FRF) for each channel from the response that was measured. A curve could then be fit to the FRF to find the modes by selecting a frequency range for ModalVIEW to analyze and the number of modes within that range. The fit of the curve could be checked and, if the fit looked good, the mode(s) would then be added to the mode list for that test. This can be seen in Figure 6. This was repeated through the FRF until a list of modes and natural frequencies was created for each test. ModalVIEW was then used to build a model of the Super Hauler. The accelerometers were assigned to their respective nodes and degrees of freedom. The structure could then be animated with the motion and mode shape associated with each natural frequency that was found.

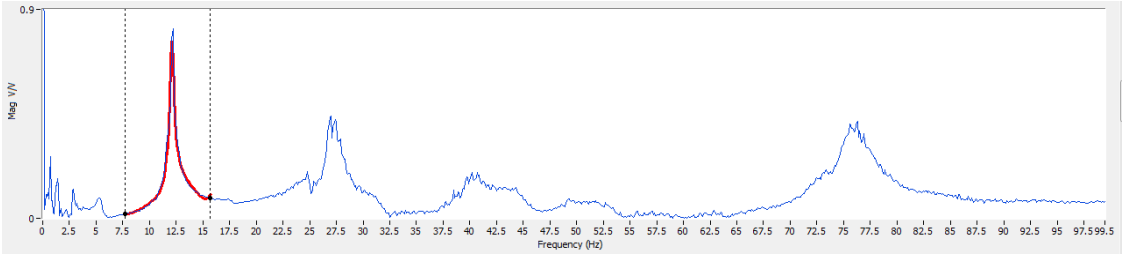

Figure 6. Sample frequency response function with curve fit on the targeted mode.

BASE MODEL

The base model consisted of a planar model of the aircraft with 12 uni-axial accelerometers and 4 tri-axial accelerometers in the locations shown in Figure 7a. All of the uni-axial accelerometers were mounted to measure acceleration in the Z direction except for the one on the vertical stabilizer, which was mounted to measure in the Y direction. The test was performed both with and without pods. When the pods were installed, four more uni-axial accelerometers were added to measure the motion of the pods. The pod accelerometer locations are shown in Figure 7b where the two on the side of the pod were mounted in the Y direction and the two on the bottom of the pod were mounted in the Z direction.

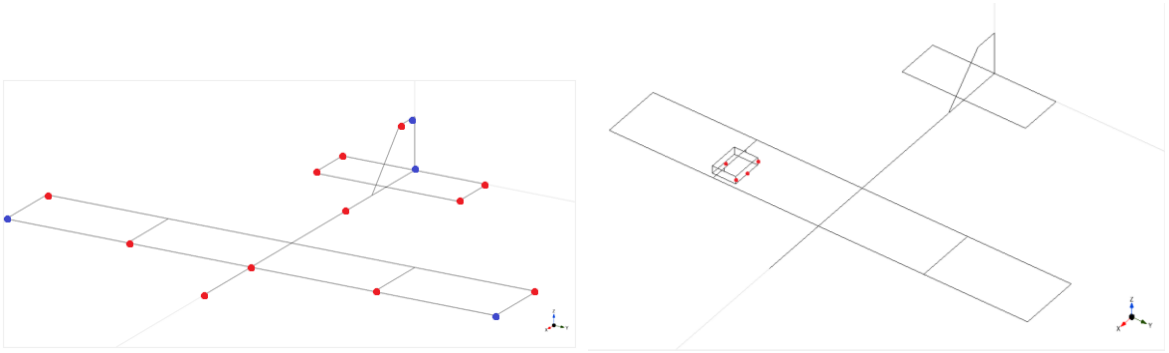

(a) (b)

Figure 7. Base model accelerometer locations (red = uni-axial, blue = tri-axial).

Figure 8 shows the mode shapes that were found and lists the corresponding natural frequencies without the pods and with the pods. The first mode shape that was observed was mode 1 type bending in the wings. The second mode shape consisted of tail torsion while the wingtips bent in opposite directions of each other. The third mode shape showed wingtip, wing, tail, horizontal stabilizer, and vertical stabilizer torsion while the wingtips also bent. The fourth mode shape only appeared in the no pods configuration and consisted of wing torsion while the horizontal stabilizer bent slightly. The fifth mode shape showed wing torsion in the same direction. The sixth mode shape showed the wingtips bending in opposite directions of each other while the tail moved side to side and the horizontal stabilizer underwent torsion and bending. The seventh mode shape showed the wingtips bending in opposite directions of each other while the tail moved side to side. The eighth mode shape only appeared in the no pods configuration and showed horizontal and vertical stabilizer torsion. The ninth mode shape only appeared in the no pods configuration and showed the horizontal stabilizer under bending and torsion with mode 2 bending in the wings and vertical stabilizer torsion. The tenth mode shape showed the wings experiencing mode 2 type bending with horizontal stabilizer bending and torsion. The eleventh mode shape showed wing and horizontal stabilizer torsion in the same direction. The twelfth mode shape only appeared with the pods and showed the wings in torsion and the horizontal stabilizer in bending and torsion. The thirteenth mode shape showed wing torsion in opposite directions from each other while the horizontal stabilizer and the body both bent. The fourteenth mode shape showed wing mode 2 bending and torsion with horizontal stabilizer torsion. The fifteenth mode shape showed horizontal stabilizer torsion while the wings underwent mode 2 wing torsion.

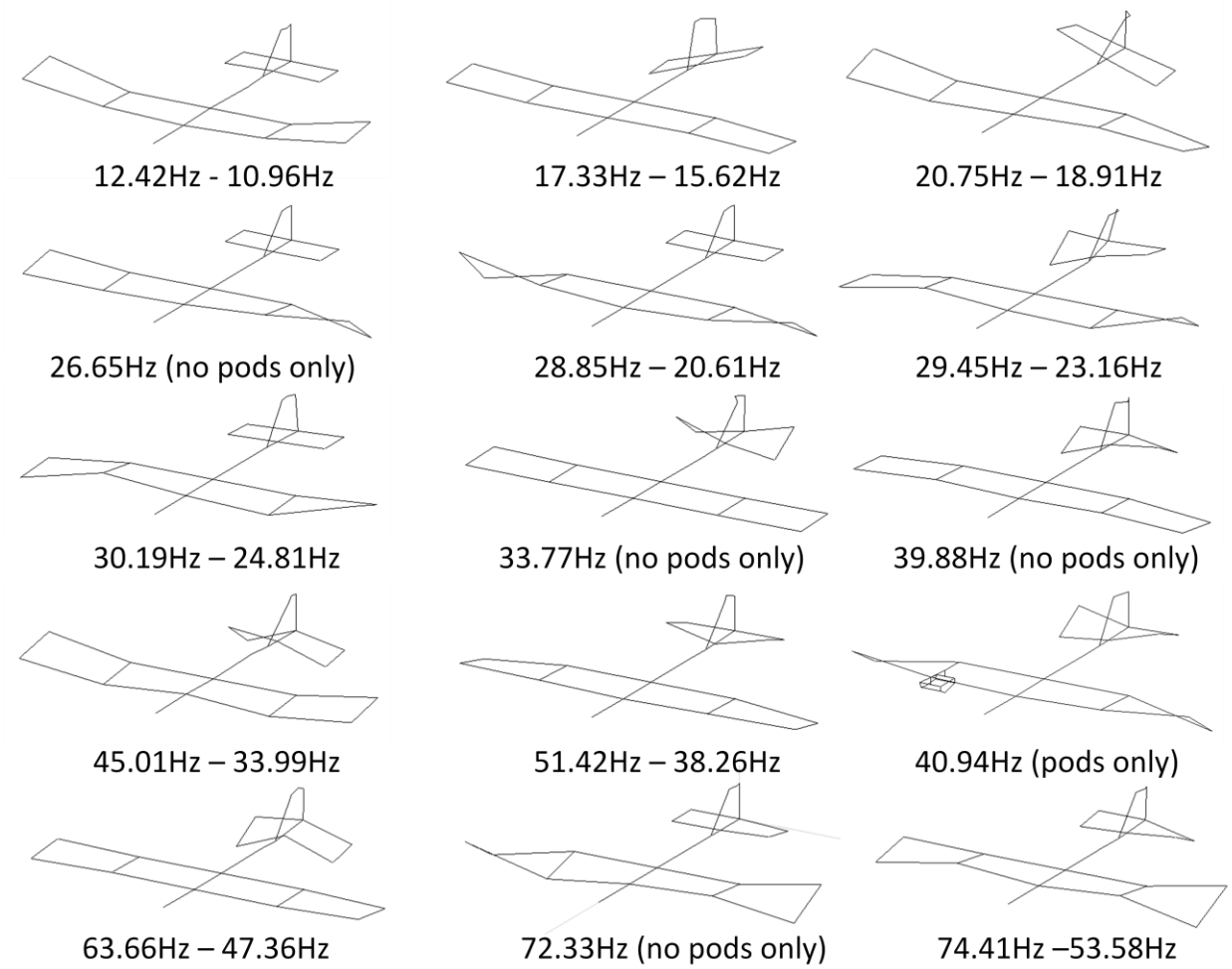

Figure 8. Base model mode shapes and natural frequencies.

The results are summarized in Table 2. It can be seen that the natural frequencies with the pods are 8%-30% smaller than the corresponding natural frequencies without pods. This was expected since, when installed, the wing pods account for 20% of the total weight of the aircraft.

Table 2. Summarized natural frequencies for the base model with and without pods.

No Pods	Pods	%Diff	Description
12.42	10.96	11.69	Mode 1 wing bending
17.33	15.62	9.89	Tail torsion, wingtip bend opposite
20.75	18.91	8.88	Wingtip, wing, tail, HS, VS torsion, wingtip bend
26.65			Wing torsion, slight HS bend
28.85	20.61	28.58	Wing torsion in same direction
29.45	23.16	21.37	Wingtips bend opposite, HS bend/torsion, tail wag
30.19	24.81	17.81	Wingtips bend opposite, tail wag
33.77			HS, VS torsion
39.88			HS bend/torsion, mode 2 wing bend, VS torsion
45.01	33.99	24.48	Mode 2 wing bend, HS bend/torsion, VS torsion
51.42	38.26	25.58	Wing torsion, HS bend/torsion
	40.94		Mode 2 wing torsion, HS bend/torsion
63.66	47.36	25.61	Wing torsion opposite, HS bend, body bend
72.33			Mode 2 wing bend, torsion opposite, HS torsion
74.41	53.58	27.99	HS torsion, mode 2 wing torsion

SENSOR LOCATION IDENTIFICATION METHOD AND CHANNEL REDUCTION

Channel reduction is an important topic in modal analysis. With every extraneous channel there are associated costs. These costs include an extra sensor and the time spent installing, indexing, and logging the sensor as well as processing and analyzing the data obtained from said accelerometer. Because of this, it is important to use as few channels as possible while still keeping enough to identify the modes of the structure [7]. A key point in channel reduction is sensor location selection. Several methods for identifying important locations for sensors have been developed.

One methodology uses a finite element model in which sensor sets are found which maximize the ability to observe modes while constraining each sensor to contribute unique information [8]. Another method selects sensor locations that make the corresponding target mode shape partitions as linearly independent as possible while maximizing the signal strength of the target modal responses within the sensor data [9]. Yet another method uses a genetic algorithm to identify sensor locations by starting with a relatively small number of possible final locations and evolving these locations to the best set [10].

There are several more methods for sensor location identification but the majority of them require extensive finite element modeling, algorithm development, mathematical modeling, or a combination thereof [11]. It was desired to develop a relatively quick and easy, non-contact, experimental method with which to identify important sensor locations for complex systems that are difficult and time consuming to model. This was achieved through the use of a laser vibrometer. A laser vibrometer is a good tool to use for this purpose because of its mobility and its capability to gather vibration data in a non-contact manner. The laser vibrometer was used to measure the velocity of the surface of the aircraft at several locations. These values were then used to identify locations of high interaction.

The laser vibrometer that was used for the tests was a Polytech OFV 2601 Laser Vibrometer Controller with a Polytech CLV Laser Unit and a Polytech CLV 700 Laser Head. To perform the laser vibrometer testing, the Super Hauler was placed in the test rig and the shaker was attached in the location marked by the blue dot in Figure 9b. The Super Hauler was in the no pods and unloaded condition.

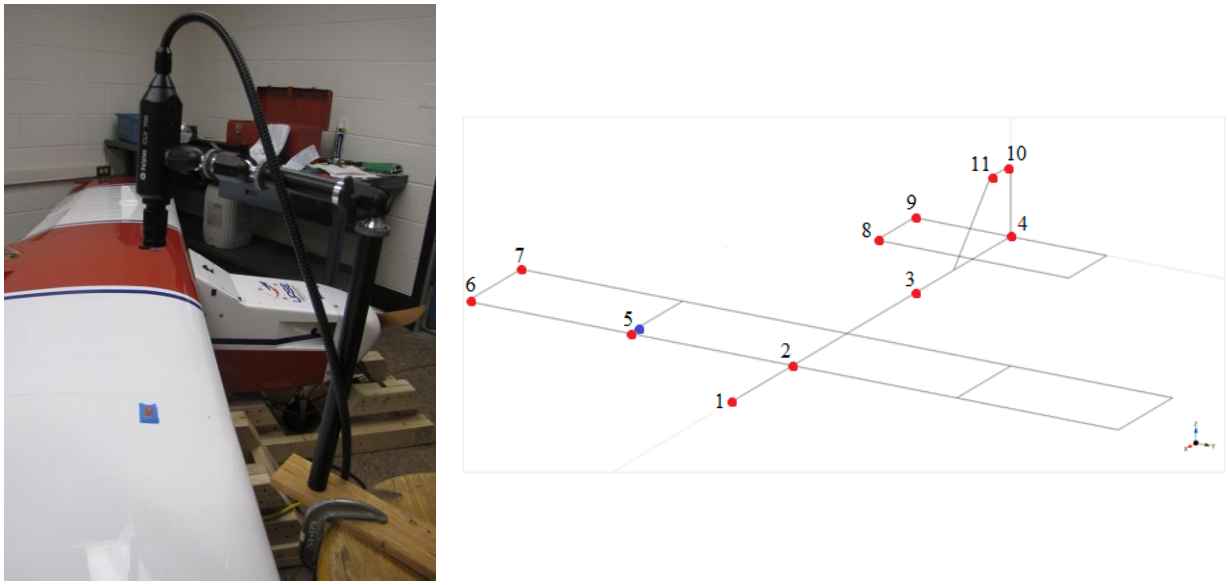

(a) (b)

Figure 9. (a) Laser vibrometer testing setup (b) Excitation (blue) and measurement (red) locations for laser vibrometer tests.

The laser vibrometer was mounted on a stand and directed to measure the vibration of the aircraft at the locations shown in Figure 9b. All measurements were in the Z direction except for the two on the vertical stabilizer which were in the Y direction. The first step in the test procedure was to move the laser vibrometer to a measurement location and focus the laser to get a strong, clear signal. Next, the shaker was activated to vibrate the aircraft with random excitation. A LabVIEW program was then run that recorded and logged the data from the vibrometer over a ten second period. These steps were repeated until three sets of data were gathered from each measurement location.

A sample of the data gathered is shown in Figure 10a. The graph shows the voltage measurements taken by the laser vibrometer of a test location versus time with the voltage corresponding to amplitude. As can be seen, the data wasn't centered around zero and there were some outliers due to noise in the laser vibrometer. Post processing was performed in Excel to remove the outliers and then shift the data sets so that they had an average of zero. The sample data set after post processing can be seen in Figure 10b.

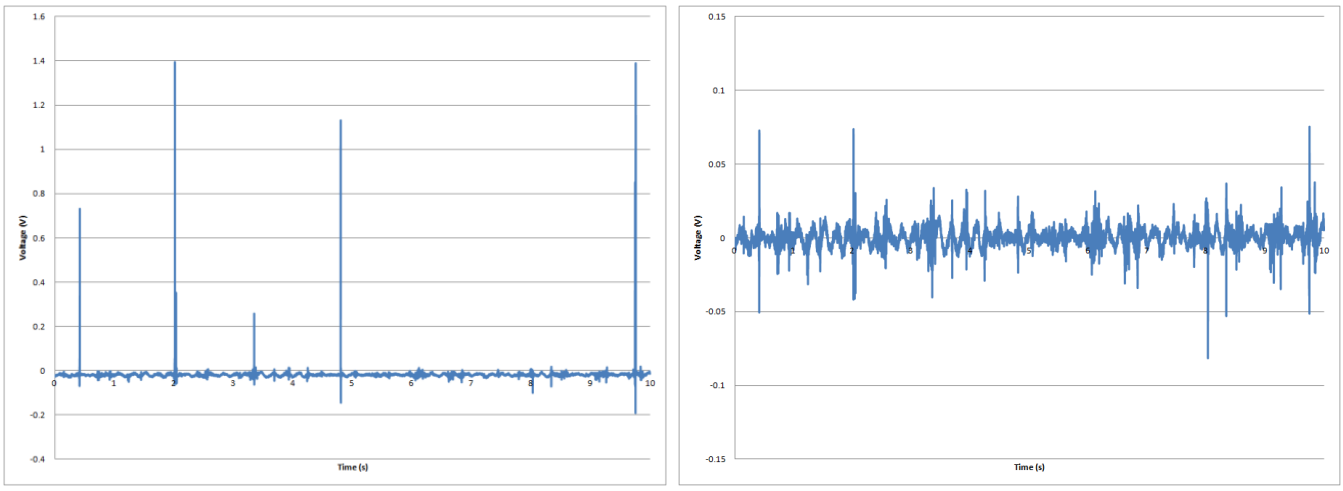

(a) (b)

Figure 10. (a) Raw laser vibrometer data. (b) Data with outliers removed and adjusted for an average of zero.

To find an effective measure of the magnitude of vibration at each location, Equation (2) was used to calculate the Root Mean Square (RMS) value for each data set.

$$x_{rms} = \sqrt{\frac{1}{n}({x_1}^2 + {x_2}^2 + \cdots + {x_n}^2)} \quad (2)$$

A representative RMS value for each measurement location was then found by calculating the average of the three RMS values from the three data sets at each location. The average RMS values at each node can be seen in Figure 11a.

Once the average RMS values were calculated, it was desirable to establish a statistical method to select the important modes at which accelerometers need to be placed. The method that was selected was a Pareto diagram. Pareto diagrams were introduced in the field of quality control and are used to determine the most significant aspects of a body of information [12]. Resources can then be used on the important aspects and not wasted on trivial aspects. The Pareto diagram method was applied to this test by first assuming the important motion of the aircraft was captured by the measured locations. Selecting the measurement locations is an important step in this process since a location has to be measured to be included in the analysis of important sensor placement locations. The average RMS values were then ordered from largest to smallest and the individual percentages of the total were calculated. These percentages were then summed to find a running cumulative percentage of total aircraft motion captured. These results were then graphed and are shown in Figure 11b where the blue bars are individual percentages of the total, and the red line is the cumulative percentage. A thorough screening of potential sensor locations must be conducted to help ensure that all the motion of interest is captured. The use of a laser vibrometer makes this process effective due to the efficiency of data collection.

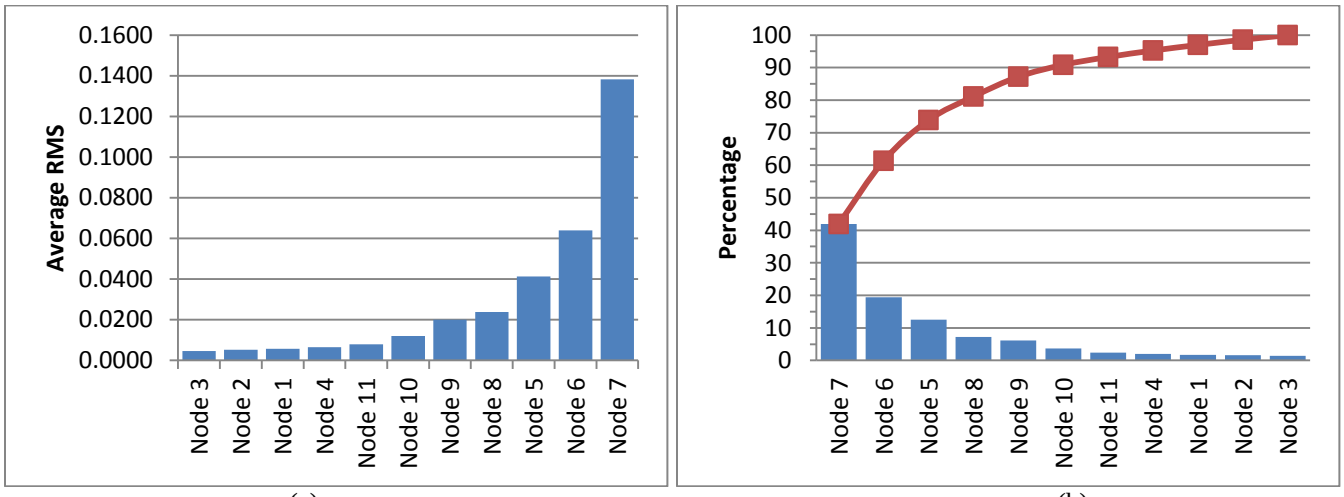

(a) (b)

Figure 11. (a) Average RMS values for laser vibrometer measurement locations and (b) Pareto diagram.

This Pareto diagram can be used to determine which locations should be measured. To capture 75% of the motion, nodes 5, 6, and 7, which are the nodes on the wings, should be instrumented. Alternatively, to capture 90% of the motion, nodes 8 and 9, on the horizontal stabilizer, would have to be instrumented as well. To capture even more motion, nodes 10 and 11 on the vertical stabilizer could be instrumented as well to bring the measured motion up to 95%. The values chosen in this case were chosen because they coincide with the various surfaces of the aircraft. Since the correct level is case dependent, this value should be left to user discretion. To examine the effects of channel reduction, tests were performed with these levels. A summary of the natural frequencies and mode shapes found in the channel reduction tests compared to the natural frequencies for the base model with no pods can be seen in Table 3.

Table 3. Summary of natural frequencies for channel reduction tests.

Base	95%	90%	75%	Description
12.42	12.40	12.40	12.40	Mode 1 wing bending
17.33	17.47	17.48	17.52	Tail torsion, wingtip bend opposite
20.75	20.80	20.79	20.96	Wingtip, wing, tail, HS, VS torsion, wingtip bend
26.65	25.99	26.01	25.87	Wing torsion, slight HS bend
28.85	28.17	28.14	28.10	Wing torsion in same direction
30.19	30.82	30.82	30.71	Wingtips bend opposite, tail wag
33.77	36.49	36.11		HS, VS torsion
39.88	39.70	39.83	39.80	HS bend/torsion, mode 2 wing bend, VS torsion
45.01	44.93	44.93	44.67	Mode 2 wing bend, HS bend/torsion, VS torsion
51.42	51.00	51.73	50.58	Wing torsion, HS bend/torsion
63.66	61.06	62.86	64.08	Wing torsion opposite, HS bend, body bend
72.33	73.27	71.97	71.87	Mode 2 wing bend, torsion opposite, HS torsion
74.41	75.92	75.88	75.76	HS torsion, mode 2 wing bend and torsion

It can be seen that the 95% test captured all of the natural frequencies that were seen in the base model. However, as would make sense from the data that was removed, any motion in the fuselage was undetectable using the 95% data. There was relatively little activity in the fuselage when compared to the rest of the structure, though, so the inability to observe that motion is fairly insignificant. The 90% test also captured all of the natural frequencies that were seen in the base model. However, any motion in the fuselage or vertical stabilizer was undetectable using the 90% data. Depending on the application, the inability to observe this motion could be acceptable since the fuselage and vertical stabilizer don't experience much motion and all of the modes were detected. The 75% test captured almost all of the natural frequencies that were seen in the base model, missing one mode at 33.77 Hz. However, any motion in the body or tail was undetectable using the 75% data. The inability to detect a mode at 33.77 Hz can be traced to this fact since that mode consists solely of horizontal and vertical stabilizer motion. This is a significant lack of data because of the inability to detect a mode. It also factors into airworthiness determinations because of the inability to see motion in the horizontal stabilizer. One important note in the data analysis is as sensors are removed, the relative magnitudes in the FRFs can change, introducing a potential for identifying modes that hadn't been recognized before or missing modes that had been previously identified.

DETERMINATION OF AIRWORTHINESS

One of the main reasons that a ground vibration test on the Super Hauler was conducted was to determine if the aircraft was still airworthy after the addition of wing pods. A major concern in aircraft is aeroelastic flutter. Aeroelastic flutter is defined as involving the interaction of aerodynamic, elastic, and inertia forces on structures that produces an unstable oscillation that often results in structural failure [13]. Flutter is typically observed on surfaces, such as wings and tails, that encounter large aerodynamic loads [14]. Flutter occurs when the aerodynamic forces associated with motion in two modes of vibration (i.e. wing bending/torsion) cause the modes to couple adversely [15]. An uncontrolled increase in vibration amplitude is observed when the aircraft is moving fast enough that the structural damping is insufficient to quell the motion coming from aerodynamic energy being added to the surface [16].

New aircraft are put through rigorous testing to identify flutter. These tests include both ground vibration tests and flight tests that include structural excitation, response measurement, and data analysis for stability [13]. The Super Hauler had been flown for several missions prior to the development of the wing pods so the stability of the aircraft had been established. The tests were performed to see if the addition of the wing pods changed the modes of the aircraft to the extent that flutter would be introduced in normal flight operations.

The primary location on an aircraft where flutter is a concern is the wings. The natural frequencies were examined to see if the addition of the pods changed the frequencies so that a wing bending mode would coincide with a wing torsional mode. Table 4 summarizes the modes that were dominated by wing motion and it can be seen that none of the frequencies aligned so that flutter conditions were created.

Table 4. Summary of wing modes.

No Pods	Pods	Description
12.42	10.96	Mode 1 wing bending
28.85	20.61	Wing torsion in same direction
29.45	23.16	Wingtips bend opposite, HS bend/torsion, tail wag
30.19	24.81	Wingtips bend opposite, tail wag
45.01	33.99	Mode 2 wing bend, HS bend/torsion, VS torsion
51.42	38.26	Wing torsion, HS bend/torsion
63.66	47.36	Wing torsion opposite, HS bend, body bend

The modes that were observed to contain potential for flutter with a combination of bending and torsional modes were noticed in the horizontal stabilizer and are summarized in Table 5. As flight loadings are smaller on the horizontal stabilizer, flutter is not as significant of a problem on this surface. However, this discovery will lead to the UASE lab increasing the tension in the stabilizer wires to combat the flutter tendencies shown in the horizontal stabilizer.

Table 5. Summary of potential horizontal stabilizer flutter modes.

No Pods	Pods	Description
29.45	23.16	Wingtips bend opposite, HS bend/torsion, tail wag
39.88		HS bend/torsion, mode 2 wing bend, VS torsion
45.01	33.99	Mode 2 wing bend, HS bend/torsion, VS torsion
	40.94	Mode 2 wing torsion, HS bend/torsion

The Super Hauler was flown in July 2012 with the wing pods attached. Dummy weights were placed in the pods to simulate a payload. The weights added brought the total weight of the pods to 5 lbs each. An image that was taken during the flight in which the pods are visible is shown in Figure 12. The flight was successful with no problems during flight and there was no noticeable change in the flight characteristics or the handling of the aircraft.

Figure 12. The Super Hauler in flight with the wing pods installed.

CONCLUSION

A full modal analysis investigating the effect of wing pods on a small UAS was presented. The pods were shown to lower the natural frequencies for corresponding mode shapes but no wing flutter was introduced into the system. This lead to the conclusion that the wing pods were a safe addition to the aircraft, which was demonstrated by a successful flight with the wing pods installed. A novel channel reduction method, using a laser vibrometer, was presented. This method was shown to provide a quick, non-contact, and experimental way to determine important sensor locations through the use of a Pareto diagram. This method provides the user with the flexibility to determine the level of information they desire to capture. A study was done on channel reduction and three different tests were performed and analyzed. The sensors along the body of the aircraft, as well as on the vertical stabilizer, were found to be unnecessary for this testing while the sensors on the wings were imperative.

ACKNOWLEDGEMENTS

This research was supported in part by Department of Defense contract number FA4861-06-C-C006 “Unmanned Aerial System Remote Sense and Avoid System and Advanced Payload Analysis and Investigation,” the Air Force Research Laboratory, “MEMS Antenna for Wireless Communications Supporting Unmanned Aerial Vehicles in the Battlefield," and the North Dakota Department of Commerce, “UND Center of Excellence for UAV and Simulation Applications.” The authors would like to also acknowledge the contributions of the Unmanned Aircraft Systems Laboratory team at UND.

REFERENCES

[1] J. Alme, *Vivaldi Antenna Design for X Band Electronically-Steered Antenna Arrays and Phased Array Radars,* University of North Dakota: Department of Electrical Engineering, 2009.

[2] D. Hajicek, *Electronically-Steered Phased Array Antenna Design for Integration Into Small Unmanned Aircraft Systems,* University of North Dakota: Department of Electrical Engineering, 2009.

[3] K. J. Lemler and W. H. Semke, "Structural Analysis of the Effects of Wing Payload Pods on Small UAS," in *30th International Modal Analysis Conference (IMAC)*, Jacksonville, Florida, February 2012.

[4] M. W. Kehoe, "Aircraft Ground Vibration Testing at NASA Ames-Dryden Flight Research Facility," National Aeronautics and Space Administration, 1987.

[5] J. Simisiriwong, *Structural Testing of an Ultralight UAV Composite Wing and Fuselage,* Mississippi State University: Department of Aerospace Engineering, 2009.

[6] D. J. Ewins, Modal Testing: theory, practice, and application, 2nd Edition, Baldock, Hertfordshire, England: Research Studies Press Ltd., 2000.

[7] T. G. Carne and C. R. Dohrmann, "A Modal Test Design Strategy for Model Correlation," in *13th International Modal Analysis Conference*, Nashville, TN, 1995.

[8] C. Stephan, "Sensor Placement for Modal Identification," *Mechanical Systems and Signal Processing,* vol. 27, pp. 461-470, 2011.

[9] D. C. Kammer and M. L. Tinker, "Optimal Placement of Triaxial Accelerometers for Modal Vibration Tests," *Mechanical Systems and Signal Processing,* vol. 18, pp. 29-41, 2004.

[10] M. Stabb and P. Blelloch, "A Genetic Algorithm for Optimally Selecting Accelerometer Locations," in *Proceedings of the 13th International Modal Analysis Conference*, 1995.

[11] C. Papadimitriou, "Pareto Optimal Sensor Locations for Structural Identification," *Computer Methods in Applied Mechanics and Engineering*, vol. 194, no. 12-16, pp. 1655-1673, April 2005.

[12] J. Lawson and J. Erjavec, Modern Statistics for Engineering and Quality Improvement, CA: Duxbury, 2001.

[13] M. W. Kehoe, "A Historical Overview of Flight Flutter Testing," National Aeronautics and Space Administration, 1995.

[14] C. De Marqui Jr., D. C. Rebolho, E. M. Belo and F. D. Marques, "Identification of flutter parameters for a wing model," *Journal of the Brazilian Society of Mechanical Sciences and Engineering*, vol. 28, no. 3, pp. 339-346, 2006.

[15] J. R. Wright and J. E. Cooper, Introduction to Aircraft Aeroelasticity and Loads, Chichester, West Sussex, England: John Wiley & Sons Ltd., 2007.

[16] C. Hebert, D. Cowan, P. J. Attar and C. D. Weisman, "Exploring Structural Dynamics," AIAA.